CHIN. PHYS. LETT. Vol. 35, No. 3 (2018) 036102

Microstructures and Mechanical Properties of $AlCrFeNiMo_{0.5}Ti_x$ High Entropy Alloys *

Zhi-Dong Han(韩志东)[1], Heng-Wei Luan(栾亨伟)[1], Shao-Fan Zhao(赵少凡)[2], Na Chen(陈娜)[1**], Rui-Xuan Peng(彭瑞轩)[1], Yang Shao(邵洋)[1], Ke-Fu Yao(姚可夫)[1**]

[1]*School of Materials Science and Engineering, Tsinghua University, Beijing 100084*
[2]*Qian Xuesen Laboratory of Space Technology, Beijing 100094*

(Received 24 October 2017)

Effects of Ti addition on the microstructures and mechanical properties of $AlCrFeNiMo_{0.5}Ti_x$ ($x = 0$, 0.25, 0.4, 0.5, 0.6, 0.75) high entropy alloys (HEAs) are investigated. All these HEAs of various Ti contents possess dual BCC structures, indicating that Ti addition does not induce the formation of any new phase in these alloys. As Ti addition x varies from 0 to 0.75, the Vickers hardness (HV) of the alloy system increases from 623.7 HV to 766.2 HV, whereas the compressive yield stress firstly increases and then decreases with increasing x above 0.5. Meanwhile, the compressive ductility of the alloy system decreases with Ti addition. The $AlCrFeNiMo_{0.5}Ti_{0.6}$ and $AlCrFeNiMo_{0.5}Ti_{0.75}$ HEAs become brittle and fracture with very limited plasticity. In the $AlCrFeNiMo_{0.5}Ti_x$ HEAs, the $AlCrFeNiMo_{0.5}$ HEA possesses the highest compressive fracture strength of 4027 MPa and the largest compressive plastic strain of 27.9%, while the $AlCrFeNiMo_{0.5}Ti_{0.5}$ HEA has the highest compressive yield strength of 2229 MPa and a compressive plastic strain of 10.1%. The combination of high strength and large plasticity of the $AlCrFeNiMo_{0.5}Ti_x$ ($x = 0$, 0.25, 0.4, 0.5) HEAs demonstrates that this alloy system is very promising for engineering applications.

PACS: 61.82.Bg, 61.50.−f, 62.20.−x, 62.20.fk, 62.20.mm DOI: 10.1088/0256-307X/35/3/036102

Recently high entropy alloys (HEAs), termed by Yeh *et al.*[1] in 2004, have received significant attention due to their unique solid solution structures and excellent mechanical properties. HEAs generally include five or more principal elements with concentrations between 5 at.% and 35 at.%. They show high strength and high hardness,[2−10] excellent corrosion resistance,[11−13] oxidation resistance[14] and wear resistance[15,16] due to multi effects of high entropy, lattice distortion, sluggish diffusion and 'cocktail'.[17,18]

The Al-Co-Cr-Cu-Fe-Ni HEAs have superior mechanical performance and have been extensively studied.[19−23] In this alloy system, Cu prefers to segregate in the interdendritic regions, leading to detrimental effects on the mechanical properties.[19,22] As a replacement, new HEA systems without containing Cu, such as AlCoCrFeNi,[23,24] $AlCoCrFeNiTi_x$,[2] $AlCoCrFeNiMo_x$,[5] $AlCoCrFeNiSi_x$,[25] $AlCoCrFeNiC_x$,[26] and $AlCoCrFeNiNb_x$[27] were developed. Among these reported systems, the $AlCoCrFeNiMo_x$ HEAs possess potentials for high-temperature engineering applications. So far, the microstructures and mechanical properties of $Al_xCoCrFeNiMo_{0.5}$, $AlCo_xCrFeNiMo_{0.5}$, $AlCoCr_xFeNiMo_{0.5}$, $AlCoCrFe_xNiMo_{0.5}$ and $AlCoCrFeNi_xMo_{0.5}$ HEAs have been investigated.[16,28−31] However, the Al-Co-Cr-Fe-Ni-Mo alloy system has poor ductility that greatly limits their engineering applications.[5] By removing the element of Co, the $AlCrFeNiMo_x$ HEAs possess better ductility than those Al-Co-Cr-Fe-Ni-Mo alloys.[3] In particular, the $AlCrFeNiMo_{0.5}$ alloy possesses the relatively high yield strength of 1748.6 MPa and large plastic strain of 12.6%.

The Al-Cr-Fe-Ni alloys possess a dual phase structure, which consists of a B2 intermetallic phase enriched in Al, Ni elements and a solid solution BCC phase enriched in Fe, Cr elements.[3,4] It is interesting to find out how the two phases evolve and interplay in the HEA alloys. Additionally, the effect of each phase on the mechanical properties of the alloys remains unclear and needs to be further studied. In the present work, the $AlCrFeNiMo_{0.5}$ alloy is selected as the base alloy due to its superior mechanical properties. The effects of Ti addition on the microstructures and mechanical properties of the $AlCrFeNiMo_{0.5}Ti_x$ alloys have been investigated.

The $AlCrFeNiMo_{0.5}Ti_x$ ($x = 0$, 0.25, 0.4, 0.5, 0.6, 0.75) HEAs were prepared by arc melting of the mixture of pure metal constituents under a Ti-gettered argon condition. Corresponding to different x, the as-prepared alloys were named as Ti0, Ti0.25, Ti0.4, Ti0.5, Ti0.6 and Ti0.75, respectively. The purities of Al, Cr, Fe, Ni, Mo and Ti exceed 99.9 wt%. To ensure the homogeneity, each ingot was re-melted four times. The ingots were cut into appropriate shapes for investigating their microstructures and mechanical properties.

The structures of the samples were characterized by x-ray diffraction (XRD, Rigaku D/max-RB) using a Cu Kα radiation. The morphology and chemical composition of the polished flat cross sections cut from the HEAs were examined by a Quanta 200 FEG scanning electron microscope (SEM) and a JOEL-2011 transmission electron microscope (TEM). SEM specimens were polished and then etched in a Kroll's Reagent of $HF:HNO_3:H_2O$=2:6:92 at room temperature. TEM samples were prepared by twin-jet electro-polishing using a mixed solution

*Supported by the National Natural Science Foundation of China under Grant No 51571127.
**Corresponding author. Email: chennadm@mail.tsinghua.edu.cn; kfyao@tsinghua.edu.cn
© 2018 Chinese Physical Society and IOP Publishing Ltd

of $HClO_4$:C_2H_5OH=1:9 with a current of 40 mA at a temperature of −25℃.

The dimensions of the samples for mechanical tests are $\Phi 3\,\text{mm} \times 6\,\text{mm}$. A WDW-50 testing machine was employed to measure the room-temperature mechanical properties of the as-prepared alloys at a strain rate of 5.6×10^{-4} s. The Vickers hardness (HV) tests of all alloys were carried out by MH-3 Vickers hardness tests with a load of 500 g and loading time of 5 s.

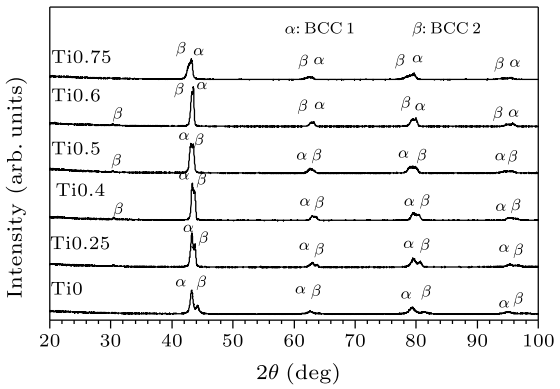

Fig. 1. XRD patterns of as-cast $AlCrFeNiMo_{0.5}Ti_x$ alloys.

Figure 1 shows the XRD patterns of the as-cast $AlCrFeNiMo_{0.5}Ti_x$ alloy samples. All of the $AlCrFeNiMo_{0.5}Ti_x$ alloys exhibit a dual-phase structure of two body-centered cubic (BCC) phases (denoted as α and β). The appearance of a (100) peak in the β phase indicates that the β phase is an order phase. The detailed structures corresponding to the two phases are further studied by TEM observations and will be given in the following. The α phase is identified as the FeCr-type disorder BCC phase, and the β phase is the NiAl-type B2 intermetallic phase. The lattice constants of the α and β phases of the Ti0 alloy are 0.297 nm and 0.291 nm, respectively. With Ti addition, the lattice constants of the β phase increase and the peak of the β phase shifted to the left accordingly. As the Ti content increases to 0.75, the lattice constants of the α and β phases in the Ti0.75 alloy are 0.297 nm and 0.298 nm, respectively.

Several parameters have been proposed to predict the structure of HEAs. Zhang *et al.* introduced a factor of Ω combining the important roles of entropy, enthalpy and atomic size difference,[32] which is defined as

$$\Omega = \frac{T_\text{m}\Delta S_\text{mix}}{|\Delta H_\text{mix}|}, \quad T_\text{m} = \sum_{i=1}^{n} c_i (T_\text{m})_i, \tag{1}$$

where ΔH_mix is the enthalpy of mixing, ΔS_mix is the entropy of mixing, $(T_\text{m})_i$ is the melting temperature of the ith element, and c_i is the atomic percentage of the ith element. They proposed that an Ω above 1.1 is required for solid solution formation.[32]

Liu *et al.* also studied the effect of atomic size difference on the HEAs.[33] Furthermore, they extended the Hume–Rothery rules for the binary alloys to the prediction of the phase formation for the HEAs. They presented the ratio γ between the smallest and largest atoms as

$$\gamma = \left(1 - \sqrt{\frac{(r_\text{S}+\bar{r})^2 - \bar{r}^2}{(r_\text{S}+\bar{r})^2}}\right) \Big/ \left(1 - \sqrt{\frac{(r_\text{L}+\bar{r})^2 - \bar{r}^2}{(r_\text{L}+\bar{r})^2}}\right),$$
$$\bar{r} = \sum_{i=1}^{n} c_i r_i, \tag{2}$$

where r_i is the atomic radius of the ith element, r_S and r_L are smallest and largest atomic sizes, and c_i is the atomic percentage of the ith element. They suggested that γ with values smaller than 1.175 is required for solid solution formation in HEAs.[33]

In addition, Liu found that the BCC phase is more stable when valance electronic concentration (VEC) is smaller than 6.87,[34] where

$$\text{VEC} = \sum_{i=1}^{n} c_i (\text{VEC})_i, \tag{3}$$

where $(\text{VEC})_i$ is the valance electron concentration of the ith atom, and c_i is the atomic percentage of the ith element.

Table 1. Parameters of Ω, γ and VEC for the $AlCrFeNiMo_{0.5}Ti_x$ HEAs.

Alloys	Ω	γ	VEC
Ti0	1.98	1.169	6.67
Ti0.25	1.73	1.196	6.53
Ti0.4	1.62	1.195	6.45
Ti0.5	1.55	1.195	6.4
Ti0.6	1.50	1.195	6.35
Ti0.75	1.43	1.194	6.29

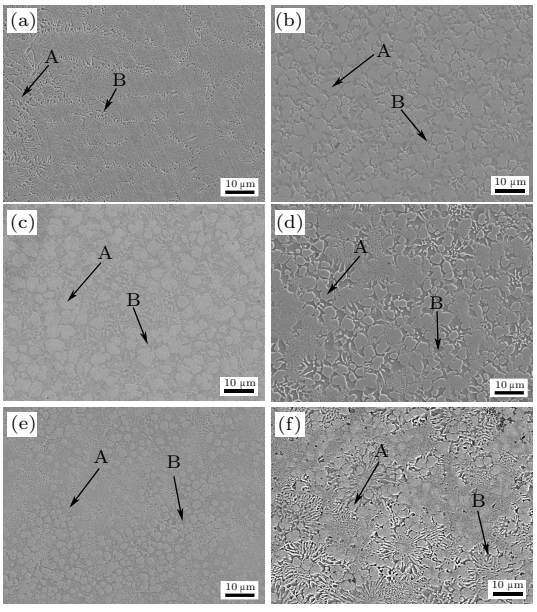

Fig. 2. SEM images of the $AlCrFeNiMo_{0.5}Ti_x$ alloys: (a) $x = 0$, (b) $x = 0.25$, (c) $x = 0.4$, (d) $x = 0.5$, (e) $x = 0.6$, and (f) $x = 0.75$.

With the increase of Ti content, Ω decreases gradually from 1.98 to 1.43, γ first increases from 1.169 for Ti0 alloy to 1.196 for Ti0.25 alloy, and then decreases to 1.194 for Ti0.75 alloy. Moreover, VEC slightly decreases from 6.67 for Ti0 alloy to 6.29 for Ti0.75 alloy with Ti alloying. According to the values of the parameters mentioned above, the Ti0 alloy should form

a single BCC solid solution structure. However, B2 and BCC phases coexist in Ti0 alloy. Thus neither of the reported rules based on the above parameters for predicting phase formation is valid in the present case, which suggests that the $AlCrFeNiMo_{0.5}Ti_x$ alloy system is very unusual.

The microstructures of the $AlCrFeNiMo_{0.5}Ti_x$ alloys are analyzed by SEM observations (Fig. 2). The alloys present a hypo-eutectic structure with a primary globular region and a lamellar eutectic structure. The element distributions in different regions (marked as A and B) of the $AlCrFeNiMo_{0.5}Ti_x$ alloys are analyzed by the SEM-EDS method.

As seen in Table 2, the Mo element is enriched in the FeCr-type phase (A regions) while poor in the NiAl-type phase (B regions), and the Ti element favors the NiAl-type phase, while it is depleted in the FeCr-type phase. As seen in the XRD results, the lattice constant of the β phase increases with the Ti content, which indicates that the NiAl-type phase corresponds to the β phase and the FeCr-type phase could be the α phase. The element distributions of $AlCrFeNiMo_{0.5}Ti_x$ alloys are similar to the reported results of the Al-Cr-Fe-Ni alloy system.[3,4] With the addition of the Ti element, the size of lamellar eutectic structure increases.

Table 2. SEM-EDS results of the $AlCrFeNiMo_{0.5}Ti_x$ alloys in different regions.

Concentrations (at%)		Al	Cr	Fe	Ni	Mo	Ti
Ti0	A	14.5	28.7	26.6	13.0	17.2	0
	B	33.5	10.1	14.1	38.1	4.2	0
Ti0.25	A	12.2	29.4	28.2	13.6	13.3	3.3
	B	34.9	9.8	13.2	32.8	4.0	5.3
Ti0.4	A	14.4	25.8	23.4	11.5	20.6	4.3
	B	30.7	10.6	12.9	31.2	3.6	11.1
Ti0.5	A	11.7	29.3	22.8	8.1	20.8	7.3
	B	29.1	7.4	13.9	34.4	2.5	12.7
Ti0.6	A	13.1	27.9	24.0	9.2	19.6	6.2
	B	26.5	10.4	13.0	30.8	4.1	15.2
Ti0.75	A	12.4	28.4	22.7	10.8	19.0	6.7
	B	24.7	12.8	14.4	26.2	5.3	16.6

Table 3. TEM-EDS results of the $AlCrFeNiMo_{0.5}Ti_x$ alloys of different phases.

Concentrations (at%)		Al	Cr	Fe	Ni	Mo	Ti
Ti0	α	14.4	30.5	25.3	16.0	13.9	0
	β	34.1	5.3	11.3	48.0	1.3	0
Ti0.25	α	4.8	38.1	30.6	5.6	16.5	4.4
	β	26.8	7.1	13.3	34.7	2.0	16.1
Ti0.5	α	5.8	38.0	33.5	4.3	16.4	1.9
	β	26.4	6.3	14.0	42.1	1.8	9.5
Ti0.75	α	7.0	37.4	30.6	3.4	16.0	5.6
	β	25.1	6.2	13.6	38.9	1.1	15.1

TEM micrographs of the as-cast $AlCrFeNiMo_{0.5}Ti_x$ alloys are shown in Fig. 3. Nano-particles distribute in a matrix and the lamellar eutectic structure is observed in Fig. 3(a). The selected area electron diffraction (SAED) patterns (inset of Fig. 3(a)) indicate that both α and β phases are of BCC structures. The chemical compositions of both phases are listed in Table 3.

The primary α phase is enriched of Fe, Cr and Mo elements, while the β phase is enriched of Al and Ni elements. A large quantity of nanoparticles is observed in the matrix (Fig. 3(a)). Eutectic regions of the Ti0.25, Ti0.5 and Ti0.75 alloys are shown in Figs. 3(b)–3(d). The SAED patterns of the two phases involved in their eutectic structures indicate that both of them are BCC phases. Meanwhile, massive nanoparticles are also observed in the two phases of the Ti0.25, Ti0.5 and Ti0.75 alloys (Figs. 3(b)–3(d)). According to the present experimental results and reported data,[4] nanoparticles in α phase and β phase are nano-sized β phase and α phase, respectively. The detailed microstructural observations demonstrate that Ti addition does not induce the formation of any new phase in the as-prepared HEAs so that all of them have dual-phase structures accompanied by nanoparticles.

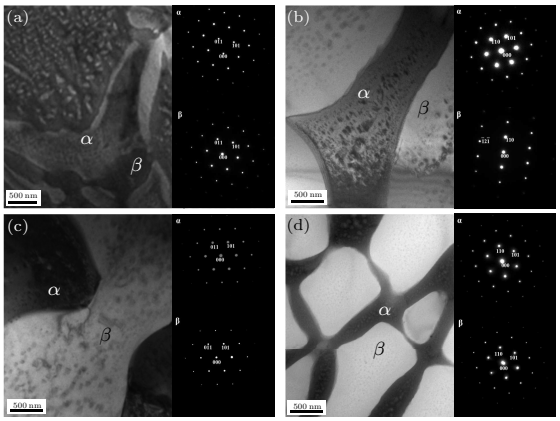

Fig. 3. TEM images of as-cast $AlCrFeNiMo_{0.5}Ti_x$ alloys: (a) Ti0, (b) Ti0.25, (c) Ti0.5, and (d) Ti0.75.

The stress-strain curves of the $AlCrFeNiMo_{0.5}Ti_x$ alloys at room temperature are shown in Fig. 4(a). The mechanical properties of all the alloys are listed in Table 4. The yield strength $\sigma_{0.2}$ of the Ti0 alloy is 1914.1 MPa, and the fracture occurs at the peak stress (σ_p) of 4023.6 MPa with the plastic strain (ε_p)

of 27.9% (Fig. 4(a)). With increasing the Ti content to 0.25, $\sigma_{0.2}$ of Ti0.25 alloy increases to 2161.7 MPa, while $\sigma_{\rm p}$ decreases to 3641.5 MPa, and $\varepsilon_{\rm p}$ decreases to 14.3%. The Ti0.4 alloy possesses $\sigma_{0.2}$ of 2185.1 MPa, $\sigma_{\rm p}$ of 3673.4 MPa, and $\varepsilon_{\rm p}$ of 14.8%. When the Ti content reaches 0.5, $\sigma_{0.2}$ of Ti0.5 is 2228.7 MPa, which is largest among the AlCrFeNiMo$_{0.5}$Ti$_x$ alloys. With the further Ti addition, the $\sigma_{0.2}$ values of the Ti0.6 and Ti0.75 alloys reduce to 1314.5 and 618.8 MPa, respectively. It is noticed that the Ti0.6 and Ti0.75 alloys are extremely brittle. The Ti element has the largest atomic radius among the constituents of the AlCrFeNiMo$_{0.5}$Ti$_x$ alloys. Inclusion of Ti thus increases the lattice distortion and improves the effect of solid solution strengthening of the HEAs. With increasing Ti contents up to 0.6 and 0.75, the lattice distortion of the B2 phase continually increases, thereby leading to increased internal stresses that make both the Ti0.6 and Ti0.75 alloys become brittle. It is noteworthy that the fracture strengths of Ti0.6 and Ti0.75 alloys are much lower than those of the other AlCrFeNiMo$_{0.5}$Ti$_x$ HEAs. Since the fracture strength could be different even for different samples with the same composition, the low fracture strengths of Ti0.6 and Ti0.75 alloys may not be intrinsic but from the flaws in the samples.

The micro-hardness values of the HEAs are displayed in Fig. 4(b). With increasing the Ti content, the hardness of the AlCrFeNiMo$_{0.5}$Ti$_x$ alloys increases from 623.7 HV for Ti0 alloy to 766.2 HV for Ti0.75 alloy (as shown in Fig. 4(b) and Table 4). The increased hardness is also caused by the solid solution strengthening.

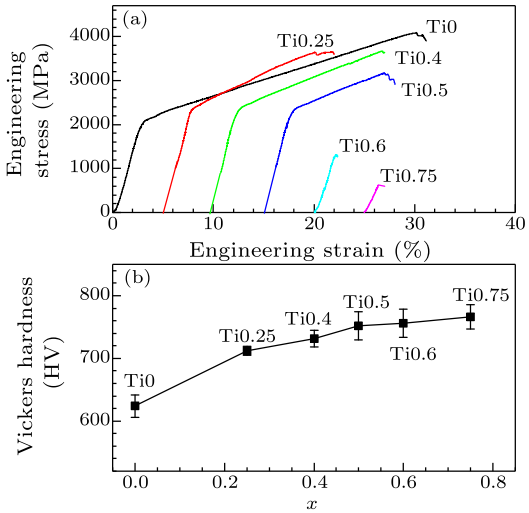

Fig. 4. Compressive engineering stress-strain curves (a) and Vickers hardness curves (b) of the AlCrFeNiMo$_{0.5}$Ti$_x$ alloys at room temperature.

Table 4. Yield strength, peak strength, plastic strain and hardness at room temperatures of the AlCrFeNiMo$_{0.5}$Ti$_x$ alloys.

Alloy	$\sigma_{0.2}$ (MPa)	$\sigma_{\rm f}$ (MPa)	$\varepsilon_{\rm p}$ (%)	Hardness (HV)
Ti0	1914.1	4023.6	27.9	623.7
Ti0.25	2161.7	3641.5	14.3	712.0
Ti0.4	2185.1	3673.4	14.8	731.9
Ti0.5	2228.7	3166.2	10.4	751.7
Ti0.6	1314.5	1314.5		756.1
Ti0.75	618.8	618.8		766.2

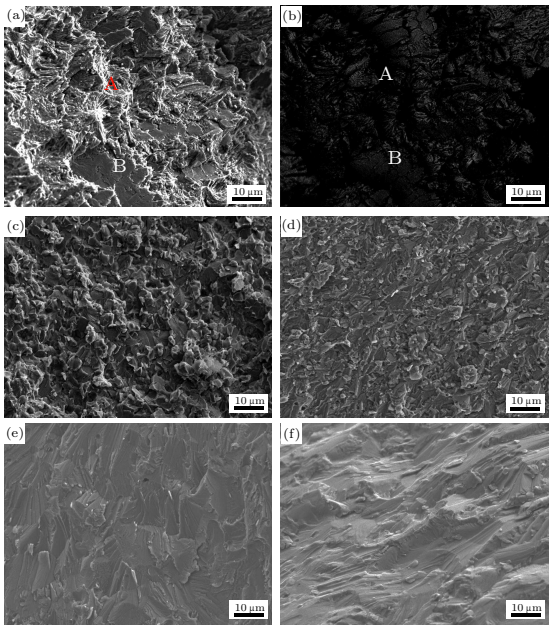

Fig. 5. SEM and BSE images of the fracture flats of AlCrFeNiMo$_{0.5}$Ti$_x$ alloys: (a) Ti0 alloy, (b) BSE image of Ti0 alloy, (c) Ti0.25 alloy, (d) Ti0.5 alloy, (e) Ti0.6 alloy, and (f) Ti0.75 alloy.

The fracture surface morphologies of the Ti0 alloy after compression tests are shown in Figs. 5(a) and 5(b). A mixture of dimple-shaped pattern (marked as A) and rough facets (marked as B) can be observed in Fig. 5(a), suggesting that the fracture mechanism of Ti0 alloy is the hybrid of both ductile and brittle fracture. The corresponding backscattered electron (BSE) image of Ti0 alloy is shown in Fig. 5(b). The dark regions in Fig. 5(b) correspond to the dimple-like pattern (A region), and the bright regions are relevant to the planar facets (B region). This indicates that the ductility of the alloys is contributed by the NiAl-type phase (β phase), while the strength is contributed by the FeCr-type phase (α phase).

As an intermetallic phase, the β phase is known to be brittle,[35] whereas it becomes ductile in the AlCrFeNiMo$_{0.5}$Ti$_x$ alloys. Such results are counter-intuitive. The increased ductility of the β phase in the AlCrFeNiMo$_{0.5}$Ti$_x$ alloys can be interpreted by the solution of Mo element in the NiAl intermetallics. Liu and Horton[35] found that the proper addition of Mo element (0.2%–3.0%) can effectively improve the ductility of the NiAl intermetallics. With the addition of Ti element, the lattice distortion of the β phase increases, which hinders the dislocation movement, and thus decreases the ductility of the AlCrFeNiMo$_{0.5}$Ti$_x$ alloy system.

The rock-candy feature shown in Figs. 5(c) and 5(d) indicates that the fracture of Ti0.25 and Ti0.5

alloys is the inter-granular fracture mode. The hybrid of river-like patterns and planar facets is shown in Figs. 5(e) and 5(f), which suggests that Ti0.6 and Ti0.75 alloys exhibit brittle transgranular fracture mode. The fracture mode transition from the inter-granular fracture to the transgranular fracture of Ti-containing $AlCrFeNiMo_{0.5}Ti_x$ HEAs suggests that the alloys become brittle with the addition of Ti.

In summary, the effects of Ti addition on the microstructures and mechanical properties of $AlCrFeNiMo_{0.5}Ti_x$ HEAs have been studied. From Ti0 to Ti0.75 alloys, the alloy system has a mixture of FeCr-type BCC phase (α phase) and NiAl-type intermetallic phase (β phase). With the increase of Ti content, the hardness of the system increases, while the yield strength increases as x varies from 0 to 0.5. When the concentration of Ti element exceeds 0.5, the alloy system becomes brittle and the yield strength decreases. Our experimental results suggest that the ductility of the $AlCrFeNiMo_{0.5}Ti_x$ HEAs is mainly contributed by the β phase, while the yield strength is mainly determined by the α phase. For Ti0.5 alloy, the yield strength, fracture strength and plastic strain are 2228.7 MPa, 3166.2 MPa and 10.4%, respectively. The superior mechanical properties of the $AlCrFeNiMo_{0.5}Ti_x$ alloys indicate that they can be potential materials for applications in the engineering field.

References

[1] Yeh J W, Chen S K, Lin S J, Gan J Y, Chin T S, Shun T T, Tsau C H and Chang S Y 2004 *Adv. Eng. Mater.* **6** 299
[2] Zhou Y J, Zhang Y, Wang Y L and Chen G L 2007 *Appl. Phys. Lett.* **90** 181904
[3] Dong Y, Lu Y P, Kong J R, Zhang J J and Li T J 2013 *J. Alloys Compd.* **573** 96
[4] Liu S, Gao M C, Liaw P K and Zhang Y 2015 *J. Alloys Compd.* **619** 610
[5] Zhu J M, Fu H M, Zhang H F, Wang A M, Li H and Hu Z Q 2010 *Mater. Sci. Eng.* A **527** 6975
[6] Ding H Y, Shao Y, Gong P, Li J F and Yao K F 2014 *Mater. Lett.* **125** 151
[7] Ding H Y and Yao K F 2013 *J. Non-Cryst. Solids* **364** 9
[8] Han Z D, Liu X, Zhao S F, Shao Y, Li J F and Yao K F 2015 *Prog. Nat. Sci.: Mater. Int.* **25** 365
[9] Zhao S F, Shao Y, Liu X, Chen N, Ding H Y and Yao K F 2015 *Mater. Des.* **87** 625
[10] Zhao S F, Yang G N, Ding H Y and Yao K F 2015 *Intermetallics* **61** 47
[11] Qiu X W, Zhang Y P and Liu C G 2014 *J. Alloys Compd.* **585** 282
[12] Li J M, Yang X, Zhu R L and Zhang Y J 2014 *Metals* **4** 597
[13] Qiu X W, Huang C X, Wu M J, Liu C G and Zhang Y P 2016 *J. Alloys Compd.* **658** 1
[14] Liu C M, Wang H M, Zhang S Q, Tang H B and Zhang A L 2014 *J. Alloys Compd.* **583** 162
[15] Chuang M H, Tsai M H, Wang W R, Lin S J and Yeh J W 2011 *Acta Mater.* **59** 6308
[16] Hsu C Y, Sheu T S, Yeh J W and Chen S K 2010 *Wear* **268** 653
[17] Yeh J W 2013 *JOM* **65** 1759
[18] Ranganathan S 2003 *Curr. Sci.* **85** 1404
[19] Tang Z, Yuan T, Tsai C W, Yeh J W, Lundin C D and Liaw P K 2015 *Acta Mater.* **99** 247
[20] Wang Y P, Li B S and Fu H Z 2009 *Adv. Eng. Mater.* **11** 641
[21] Tsai M H, Yuan H, Cheng G M, Xu W Z, Tsai K Y, Tsai C W, Jian W W, Juan C C, Shen W J, Chuang M H, Yeh J W and Zhu Y T 2013 *Intermetallics* **32** 329
[22] Yeh J W, Chen S K, Gan J Y, Lin S J, Chin T S, Shun T T, Tsau C H and Chang S Y 2004 *Metall. Mater. Trans.* A **35** 2533
[23] Wang W L, Meng L J, Li L H, Hu L, Zhou K, Kong Z H and Wei B B 2016 *Chin. Phys. Lett.* **33** 116102
[24] Qiao J W, Ma S G, Huang E W, Chuang C P, Liaw P K and Zhang Y 2011 *Mater. Sci. Forum* **688** 419
[25] Zhu J M, Fu H M, Zhang H F, Wang A M, Li H and Hu Z Q 2010 *Mater. Sci. Eng.* A **527** 7210
[26] Zhu J M, Fu H M, Zhang H F, Wang A M, Li H and Hu Z Q 2011 *J. Alloys Compd.* **509** 3476
[27] Ma S G and Zhang Y 2012 *Mater. Sci. Eng.* A **532** 480
[28] Hsu C Y, Juan C C, Sheu T S, Chen S K and Yeh J W 2013 *JOM* **65** 1840
[29] Hsu C Y, Wang W R, Tang W Y, Chen S K and Yeh J W 2010 *Adv. Eng. Mater.* **12** 44
[30] Hsu C Y, Juan C C, Wang W R, Sheu T S, Yeh J W and Chen S K 2011 *Mater. Sci. Eng.* A **528** 3581
[31] Juan C C, Hsu C Y, Tsai C W, Wang W R, Sheu T S, Yeh J W and Chen S K 2013 *Intermetallics* **32** 401
[32] Yang X and Zhang Y 2012 *Mater. Chem. Phys.* **132** 233
[33] Wang Z J, Huang Y H, Yang Y, Wang J C and Liu C T 2015 *Scr. Mater.* **94** 28
[34] Guo S, Ng C, Lu J and Liu C T 2011 *J. Appl. Phys.* **109** 103505
[35] Liu C T and Horton J A 1995 *Mater. Sci. Eng.* A **192-193** 170